Multi-Layered Avalanche Diamond Detector for Fast Neutron Applications

Project #: NLV-003-20 | Year 3 of 3

Amber Guckes,[1,a] *Robert Buckles,*[a] *Adam Wolverton,*[a] *Jesse A. Green,*[a] *Charles Han,*[b] *Kaleab Ayalew*[a,b]

[1]guckesal@nv.doe.gov, (702) 295-0199
[a]Nevada National Security Site (NNSS), North Las Vegas; [b]University of Nevada, Las Vegas

The multi-layered avalanche diamond (MAD) detector employs the intrinsic avalanche and atomic properties of single crystal chemical vapor deposition (scCVD) diamond to yield a novel fast neutron detector with inherent gain, improved detection efficiency compared to a single layer, and a small footprint. Such a device can provide an inherently low noise, high fidelity, current mode measurement of a pulsed neutron source. This measurement is critical to informing the deuterium-tritium (D-T) dense plasma focus (DPF) neutron source term in the calculation of the change in effective neutron multiplication factor, Δk_{eff}, of test objects in the NNSS Area 11 DPF campaigns and ultimately the Excalibur series of subcritical experiments (SCEs).

Background

A 500-µm-thick scCVD diamond detector with one diamond layer and two electrical contacts is currently fielded at Area 11 to measure the D-T DPF neutron pulse. It must be fielded very close to the DPF or with an external amplifier in order to obtain a measurable signal. The amplifier introduces unwanted noise and takes up space which is already limited. Additionally, the limitation on how close the detector needs to be to obtain a measurable signal eliminates the possibility of performing valuable neutron time-of-flight (nToF) measurements. The authors predicted that a scCVD diamond avalanche device with several vertically stacked layers can maintain geometrical gain similar to a photomultiplier tube (PMT) providing an increased signal-to-noise ratio and flexibility in fielding the detector further from the source.

This avalanche effect is electron-hole multiplication achieved by increasing the electric field within the scCVD diamond high enough that secondary electrons created from radiation interactions in the diamond can be kinetically accelerated beyond the band gap energy before colliding/scattering within the lattice (Knoll 2010). Fields of 30 V/µm and greater have been observed to demonstrate avalanche gain in thin diamond radiation detectors (Skukan et al. 2016; Muškinja et al. 2017). Electrons at avalanche speeds have enough energy to transit a thin metal layer (~10 nm) and can be transported between vertically stacked layers to continue producing compounded secondaries resulting in multiplicative gain (Antula 1972; Monteblanco et al. 2019). Alternatively, electrons at avalanche speeds can be transported horizontally through the bulk of the diamond creating secondary electrons yielding the same effect. In either approach, the proximity of the metal layers in a thin diamond layer is key to a sustained field in the presence of significant charge generation (Skukan et al. 2016; Muškinja et al. 2017).

Other properties of diamond bolster its attractiveness for use in radiation detection. It exhibits high radiation hardness and a 5.5 eV band gap (Kania et al. 1993) along with a FWHM [full

This work was done by Mission Support and Test Services, LLC, under Contract No. DE-NA0003624 with the U.S. Department of Energy, the Office of Defense Programs, and supported by the Site-Directed Research and Development Program. DOE/NV/03624--1692

width half maximum] on the order of 1 ns (Dueñas et al. 2015) and superior long-term stability (Knoll 2010). The high atomic density and low atomic number of diamonds translates into a high neutron detection efficiency per unit volume (Schmid et al. 2014) and limits gamma ray interaction (Kania et al. 1993; Bennett et al. 2018).

Project

The primary goal of this project was to design and fabricate a novel MAD detector leveraging the intrinsic avalanche and atomic properties of scCVD diamond to yield a novel fast neutron detector with inherent gain, improved detection efficiency compared to a single layer, and a small footprint. A series of calculations, simulations, and single-layer thin scCVD diamond detector measurements were performed to inform the MAD detector design. The data gleaned from these efforts ultimately led to the design and fabrication of two MAD detectors: one based on the transport of electrons through vertically stacked diamond layers and the other based on the horizontal transport of electrons through the bulk of a single diamond layer.

Year One: Understanding Diamond Detector Physics

Fast Neutron Interactions in Diamond

The neutron energy of interest for this work was 14.1 MeV since the DPF used in Neutron Diagnosed Subcritical Experiments (NDSE) creates neutrons at this energy. There are several neutron interactions that are possible on both ^{12}C and ^{13}C in diamond for 14.1 MeV incident neutrons. Each of these interactions and their respective microscopic and macroscopic cross section, Q-value, and kinetic energy of the resultant products, are provided in Table 1. The interactions with the highest probability of occurrence are not necessarily the interactions whose products deposit the most energy in the diamond creating the most electron-hole pairs per interaction. The four most prominent interactions of 14.1 MeV neutrons in diamond based on a consideration of both the macroscopic cross section and product kinetic energy are elastic scattering on ^{12}C, $^{12}C(n,\alpha)^{9}Be$, $^{12}C(n,n+2\alpha)^{4}He$, and $^{13}C(n,\alpha)^{10}Be$. Energy deposition from each of these interactions was confirmed with a Geant4 simulation of a 500 μm thick diamond detector. The results of this simulation are shown in Figure 1.

The neutron interactions which deposit the most energy and thus, create the most electron-hole pairs per interaction in diamond are $^{12}C(n,\alpha)^{9}Be$, $^{12}C(n,n+2\alpha)^{4}He$, and $^{13}C(n,\alpha)^{10}Be$. The energy deposited by the reaction products are 8.40, 6.83, and 10.3 MeV, respectively. The macroscopic cross sections are approximately one order of magnitude lower for all of these interactions than elastic scattering on the respective target carbon nuclei. However, when the $^{12}C(n,\alpha)^{9}Be$ and $^{12}C(n,n+2\alpha)^{4}He$ reactions do occur, the products of these reactions will deposit approximately 4.2 and 3.4 times more energy, respectively, than the recoil ^{12}C nucleus from an average elastic scattering event. Similarly, the products of the $^{13}C(n,\alpha)^{10}Be$ reaction will deposit 5.5 times more energy than the recoil ^{13}C nucleus from an average elastic scattering event on ^{13}C.

Table 1. Microscopic and **Macroscopic Cross Sections**, Q-**V**ales, and **Product Kinetic Energies** for 14.1 MeV **Neutron Interactions** on ^{12}C and ^{13}C in **Diamond**

Interaction	**Microscopic cross section, σ (barns)[a]**	**Macroscopic cross section, ∑ (cm^{-1})**	**Q (MeV)**	**$E_{products}$ (MeV)**
$^{12}C(n,el)^{12}C$	0.827	0.144	0.00	2.00 (avg.)
$^{12}C(n,inl)^{12}C^*$	0.423	0.0734	-E*[b]	E*[b]
$^{12}C(n,n+2\alpha)^{4}H$	0.203	0.0352	-7.27	6.83
$^{12}C(n,\alpha)^{9}Be$	00.0699	0.0121	-5.70	8.40
$^{13}C(n,el)^{13}C$	1.31	2.46E-03	0.00	1.87 (avg.)
$^{13}C(n,inl)^{13}C^*$	0.552	1.04E-03	-E*[b]	E*[b]
$^{13}C(n,\alpha)^{10}Be$	0.158	2.97E-04	-3.84	10.3
$^{13}C(n,n+\alpha)^{9}Be$	7.88E-3	1.48E-05	-10.6	3.46
$^{12}C(n,\gamma)^{13}C$	1.20E-4	2.08E-05	4.94	19.0
$^{13}C(n,2n+\alpha)^{8}Be$	6.17E-6	1.16E-08	-12.3	1.80
$^{13}C(n,\gamma)^{14}C$	3.92E-5	7.36E-08	8.17	22.3
$^{13}C(n,t)^{11}B$	2.22E-3	4.17E-06	-12.4	1.68
$^{13}C(n,2\alpha)^{6}Be$	9.93E-7	1.86E-09	-12.0	2.07
$^{13}C(n,n+2\alpha)^{4}He$	1.88E-15	3.53E-18	-13.0	1.14
$^{13}C(n,p)^{13}B$	7.61E-4	1.43E-06	-12.7	1.45

[a]Data from the National Nuclear Data Center (Evaluated Nuclear Data File [ENDF])
[b]The Q-values and thus, the product kinetic energies for inelastic scattering interactions, are dependent on the excitation energy of the target C nucleus.

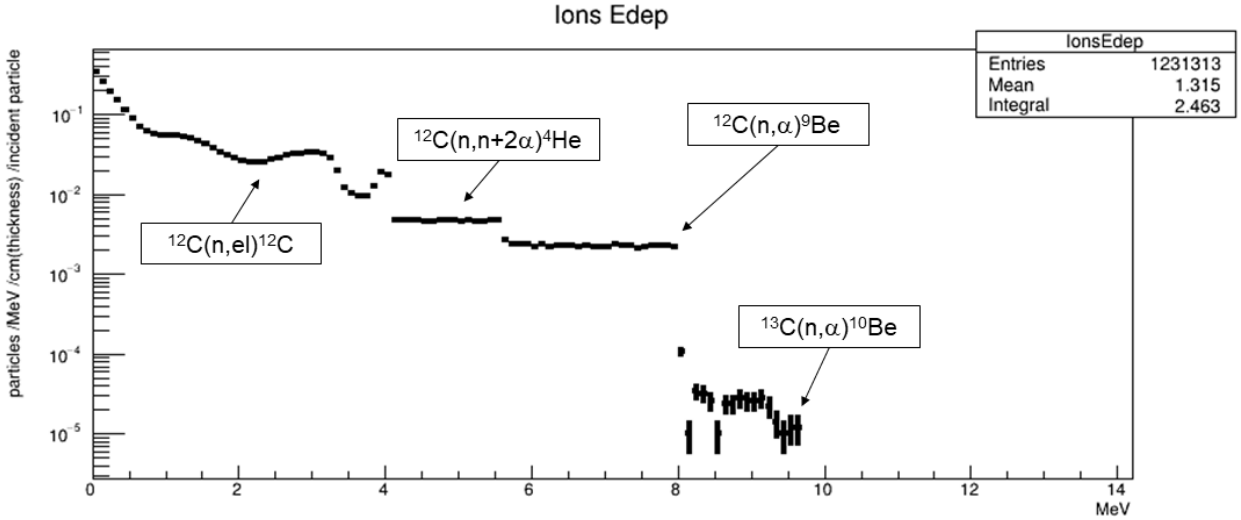

Figure 1. Geant4-simulated energy deposition spectrum from 14.1 MeV neutron interactions in a 500-µm-thick diamond detector.

Electron-Hole Creation, Transport, and the Avalanche Effect in Thin Diamond

As recoil ions and charged particles are created from neutron interactions in the diamond, they will strip valence electrons from surrounding carbon atoms, thus ionizing the atoms and leaving holes. In order for the electrons to move from the valence band to the conduction band where

they are free to be transported, they must meet a minimum energy, otherwise known as the bandgap. The bandgap for diamond is 5.5 eV (Nebel 2003).

Once the electrons are in the conduction band, they can be transported by applying an electric field. The electrons are collected on one electrode, and the holes, which are traveling in the opposite direction of the electrons, are collected on the opposite polarity electrode, assuming a sandwich-type detector configuration (i.e., one electrode on either face of the diamond layer). The ionization energy required to liberate one electron-hole pair in a semiconductor can vary based on the ionizing particle type and energy and temperature. It has been observed that approximately 13 eV deposited in the diamond by incident radiation is required to generate one electron-hole pair (Chynoweth 1958; Nebel 2003). Assuming an average energy deposited in diamond of 2.0 MeV by elastically scattered 14.1 MeV neutrons, 1.54×10^5 electron-hole pairs will be created in a single event. Conversely, the 8.4 MeV deposited by the product alpha particle and ^{9}Be ion from the ^{12}C(n,α)^{9}Be reaction will generate 6.46×10^5 electron-hole pairs in a single event.

When the electric field within a scCVD diamond is increased high enough, secondary electrons created from radiation interactions in the diamond can be kinetically accelerated beyond the bandgap energy before colliding/scattering within the lattice (i.e., the avalanche effect). We employed the empirical Chynoweth (1958) model to predict the avalanche effect in scCVD diamond. Chynoweth's work indicated that the ionization rate α of holes, and most probably electrons, is dependent on the electric field $|E|$ defined in Equation 1,

$$|E| = \frac{V}{\varepsilon \cdot d}, \tag{1}$$

where V is the applied bias voltage in volts, ε is the dielectric constant for diamond (Kania et al. 1993), and d is the diamond thickness in micrometers. Furthermore, the ionization rate as a function of the electric field could be defined by the equation shown in Equation 2,

$$\alpha = a \cdot exp\left(-\frac{b}{|E|}\right), \tag{2}$$

where a and b are empirically determined coefficients. These coefficients are different for holes and electrons, as well as different types of diamond.

Gabrysch (2010) determined two possible sets of these coefficients for holes, assuming that holes dominate the impact ionization process, in scCVD diamond by fitting the Chynoweth model to experimental data. These two sets of coefficients provided a reasonable guess for us to hypothesize pessimistically or optimistically on the Chynoweth model. For optimistic impact ionization, $a = 4 \cdot 10^6 \frac{1}{\text{cm}}$ and $b = 1.1 \cdot 10^7 \frac{V}{\text{cm}}$. For pessimistic impact ionization, $a = 6 \cdot 10^5 \frac{1}{\text{cm}}$ and $b = 0.8 \cdot 10^7 \frac{V}{\text{cm}}$.

We assume that the gain due to impact ionization, and thus the avalanche effect, is dependent on both the impact ionization rate and the diamond thickness as indicated in Equation 3. Taking the log of Equation 3, as shown in Equation 4, and multiplying the result by 20 yields the device

gain in decibels. Solving Equation 5 by substituting the aforementioned variables over a range of diamond thicknesses provides us with an initial guess of how the intrinsic avalanche effect in thin scCVD diamond translates to gain. The resulting plots are provided in Figure 2 for the optimistic impact ionization rate and Figure 3 for the pessimistic impact ionization rate.

$$\text{Gain} = 2^{\alpha d} \tag{3}$$

$$log(\text{Gain}) = log(2) \cdot \alpha \cdot d = log(2) \cdot a \cdot exp\left(\frac{b}{|E|}\right) \cdot d \tag{4}$$

$$\text{Gain in dB} = 20 \cdot log(\text{Gain}) \tag{5}$$

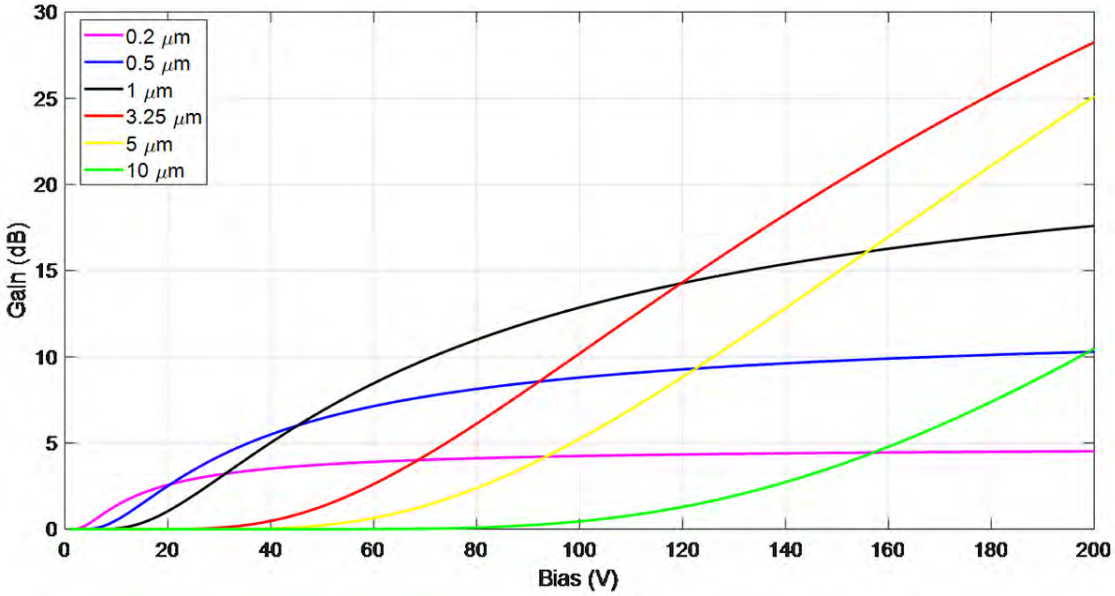

Figure 2. Avalanche gain (dB) as a function of applied bias voltage (V) and diamond thickness for the optimistic impact ionization rate calculated from Gabrysch's work

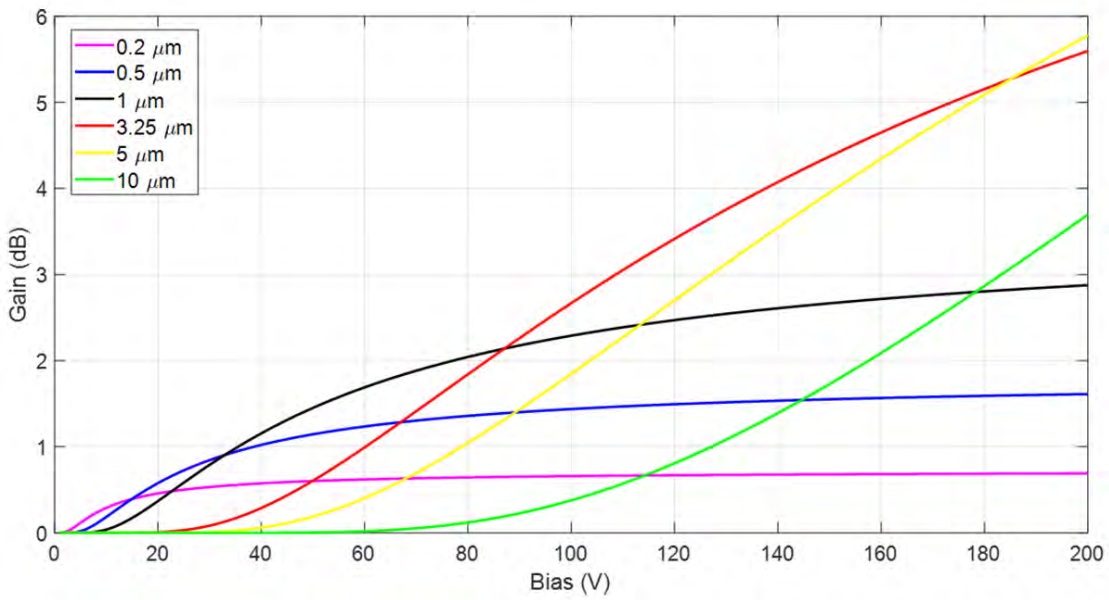

Figure 3. Avalanche gain (dB) as a function of applied bias voltage (V) and diamond thickness for the pessimistic impact ionization rate calculated from Gabrysch's work

From a conservative field breakdown perspective, we see that avalanche gain is not appreciable except for thin layers with several hundred volts of bias. This exceeds the lower observed dielectric strength of diamond previously reported. However, the dielectric strength in thin diamond samples is likely higher. If we dispense with a conservative view of breakdown and use thicker samples, we might operate with many kV across the diamond sample.

Single-Layer Thin scCVD Diamond Detector Measurements

These results, coupled with considerations for ease of fabrication, informed our decision to pursue the fabrication of two thin scCVD diamond detectors. These two detectors were employed in direct current measurements as described in the following section to corroborate our avalanche gain predictions. Working closely with Applied Diamond, Inc., we developed two thin-layered scCVD diamond detectors, one 10 and one 5 μm thick. The 10-μm-thick device is shown in Figure 4.

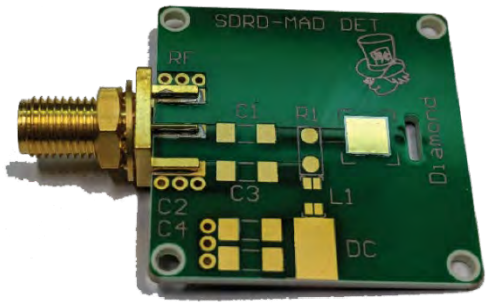

Figure 4. Single-layer, 10-μm-thick scCVD diamond detector

Direct current measurements with an electrometer were performed with both of these detectors. The neutron source used was an MP320 Thermo Fisher neutron generator. The generator was operated in continuous mode and yielded ~10^8 neutrons per second in to 4π. Both dark current (no radiation) and irradiated current (with radiation) measurements were made with each detector at each applied bias voltage. The difference between the irradiated and dark current provides the net current or offset produced from the neutron interactions in the diamond alone. The bias voltage applied to each detector was increased with the aim to observe charge multiplication while avoiding a hard breakdown.

The offset current from the 10-µm diamond detector as a function of displacement field, or the bias divided by device thickness, is shown in Figure 5. This plot reveals an exponential increase in the offset current at 20 V/µm, which is indicative of charge multiplication. Extrapolating gain values from the 10 µm diamond detector data and fitting the Chynoweth model to them yields the coefficients a = 4.63/µm and b = 8.52 V/µm. These coefficients, along with those derived from the 5-µm diamond detector data, and our optimistic and pessimistic predictions, are shown in Table 2 for comparison. We calculated the gain in decibels using these coefficients and plotted as a function of applied bias voltage in blue in the plot on the right. Our optimistic and pessimistic predictions for gain based on Gabrysch's work are shown in red and green, respectively, for comparison.

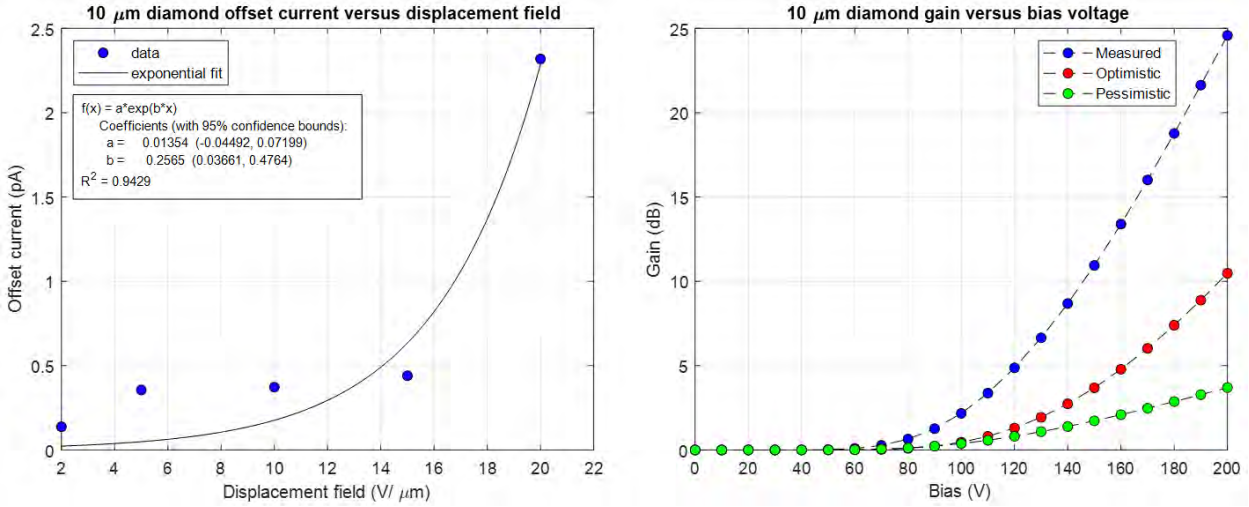

Figure 5. 10-µm-thick diamond detector offset current versus displacement field (*left*) and gain versus bias voltage (*right*).

Table 2. Comparison of Experimentally Determined Chynoweth Model Coefficients to Estimates

Fit coefficients	10-µm diamond data fit	5-µm diamond data (bias up) fit	Optimistic estimate	Pessimistic estimate
a (1/µm)	4.63	7.36	4.00	0.60
b (V/µm)	8.52	13.3	11.0	8.00

The optimistic predicted gain for the 10-µm diamond detector begins to deviate from 0 dB or unity (no units) at 90 V or 9 V/µm, and it reaches 10.5 dB at the maximum applied bias of 200 V or 20 V/µm. The pessimistic predicted gain also begins to deviate from 0 dB at 90 V or 9 V/µm, but it reaches only 3.69 dB at 200 V or 20 V/µm. The gain from our measurements begins to deviate from 0 dB at 70 V or 7 V/µm, and it reaches 24.6 dB at 200 V or 20 V/µm. The gain from our measurements indicates an improved impact ionization rate compared to either of our predictions. Variables such as detector design, diamond quality, and measurement methodology can play a role in such differences.

A slightly less prominent, yet still noticeable, increase in the offset current from the 5-µm diamond detector occurs at 15 V/µm in the data measured at increasing bias voltages. The offset current as a function of displacement field for the 5-µm diamond detector is shown in Figure 6. Extrapolating gain values from the 5 µm diamond detector data and fitting the Chynoweth model to them yields the coefficients a = 7.36/µm and b = 13.3 V/µm. Once again, we calculated the gain in decibels using these coefficients and plotted as a function of applied bias voltage in blue in the plot on the right.

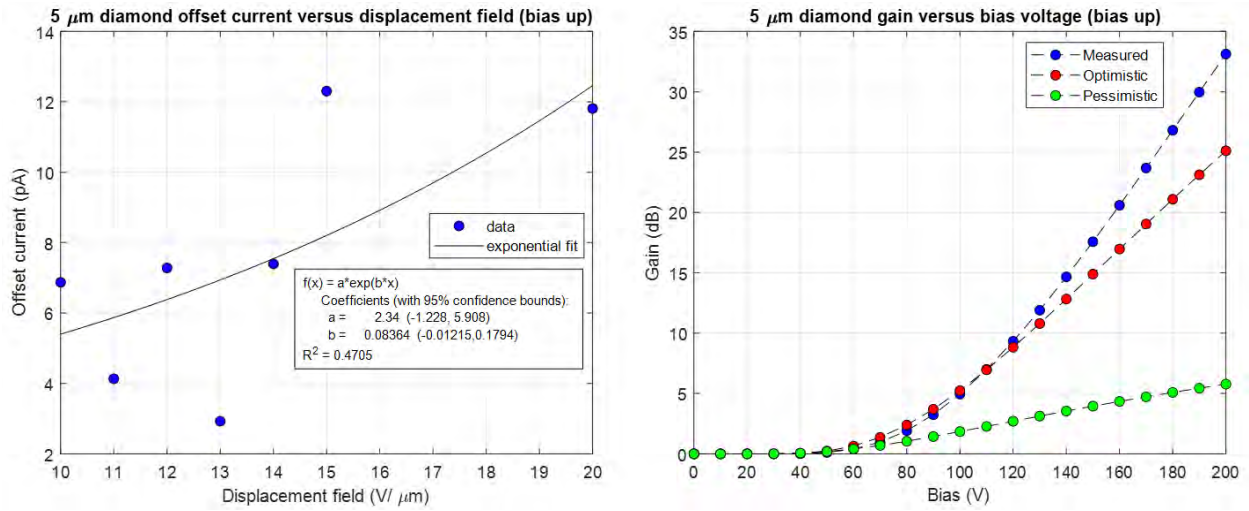

Figure 6. 5-µm-thick diamond detector offset current versus displacement field (*left*) and gain versus bias voltage (*right*). Bias voltage increased during measurements.

The gain from our measurements with the 5-µm diamond detector begins to deviate from 0 dB at approximately 60 V or 6 V/µm, and it reaches 33.1 dB at 200 V or 20 V/µm. In this case, the gain from our measurements tracks fairly well with the optimistic prediction until 140 V, where the gain from our measurements shows an improved impact ionization rate.

From our measured current data, we did observe a significant increase in current indicating charge multiplication beginning at 15 V/µm with the 5-µm-thick diamond detector and 20 V/µm with the 10-µm-thick diamond detector. We fitted the measured data to the Chynoweth model and determined impact ionization rate and ultimately gain as a function of bias voltage for each device. The gain as predicted by the Chynoweth model at the maximum bias voltage of +200 V applied to each device was 33.1 dB for the 5-µm-thick diamond detector and 24.6 dB for the 10-µm-thick diamond detector.

We were unable to resolve the dark current from the irradiated current beyond 20 V/μm due to the low number of neutrons being detected per pulse from the MP320 neutron generator. To increase the contrast, we are pursuing the use of a higher yield neutron source to increase signal. Design changes to the detector such as smaller area electrodes and/or passivation are possible solutions to decrease the leakage current. Such changes will also provide greater contrast and help avoid a hard breakdown at higher electric field values.

We also observed signs of possible charge depletion and polarization in the measured currents of both detectors. These signs were apparent when comparing the measured current with the detector biased up or down and observing the dark or irradiated current as a function of time for both detectors. The impacts of polarization and charge depletion in the diamond pose a challenge for achieving optimal charge multiplication.

Year Two: MAD Detector Design and Proof of Fabrication Processes

Based on the results of the calculations, simulations, and experimental single-layer thin scCVD diamond detector measurements performed in the first year of this project, we predicted that a multi-layer scCVD diamond avalanche device with several vertically stacked layers could maintain geometrical gain similar to a PMT and would provide an increased signal-to-noise ratio and flexibility in fielding the detector further from the source. We devised two such detector designs in the second year of this project utilizing a horizontal transport geometry in the first approach and vertical transport geometry in the second. We worked with Applied Diamond to evaluate the feasibility of fabricating either device to decide which device we would purse.

Horizontal MAD Detector Design

In the horizontal device, the full width of the diamond (~4 mm) is used as an accelerator for electrons to reach saturation velocity and keep producing secondaries until they strike the anode. However, unlike a large monolithic block of amorphous diamond, the proximate internal electrodes in this case maintain a high accelerating field in the presence of charge without intercepting the electrons. Unlike a multilayered ceramic chip capacitor, this hybrid construction is grown as single-crystal “plates,” cut to size, and lithographically processed with metal and passivation patterns. The fine metal between layers maintains the applied field in the presence of charge. The height is ultimately limited by the number and appropriate thickness of wafers. Our first horizontal device prototype included two diamond layers, although twelve are estimated to produce an acceptable neutron sensitivity volume.

Vertical MAD Detector Design

In the alternative vertical concept, diamond chips are simply stacked, with anode at the top of the stack and cathode at the bottom, with each layer biased via an ultrathin metal interface. The whole area of the diamond chips acts in parallel for increased net signal, and we are presently limited to 4 × 4 mm in scCVD diamond. We have demonstrated the compression bonding of two such layers and so, having multiple avalanche layers is a proven fabrication capability. Multiplicative gain (of order 2^N for N-layers) is achieved by high-field transport through the thin, permeable intermetal dynode interfaces and continuing acceleration into/through successive

diamond layers. We would expect there to be approximately 30 such layers for single neutron detection. However, loss is expected for any electrons born too close to the metal interfaces. These will not achieve enough energy to pass through and should be reclaimed at the metal junctions.

It should be noted that the formal design of a four-layer vertical MAD detector was prepared in the third year of this project. It was decided in the second year of this project that the horizontal MAD detector design would be pursued first as explained in the following section.

Standing-Up the MAD Detector Fabrication Process

In both horizontal and vertical approaches, the difficulty lies in the specific steps of processing the assemblies, and the vertical challenges are first being addressed in the horizontal device. Either design has some trade-off in potential losses. Ultimately, we selected the horizontal MAD detector to fabricate first. We formalized its design and awarded a subcontract to Applied Diamond to fabricate the device in mid-July 2021. Fabrication of the two-layer horizontal MAD detector continued through to the third year of this project facing and overcoming many challenges along the way.

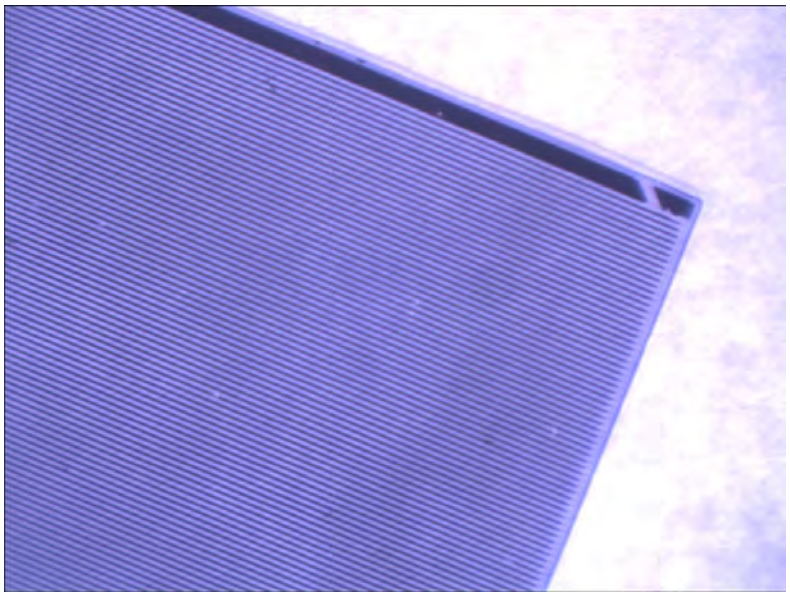

Figure 7. Sample 10-µm width and 10-µm gap electrode metallization patter on scCVD diamond

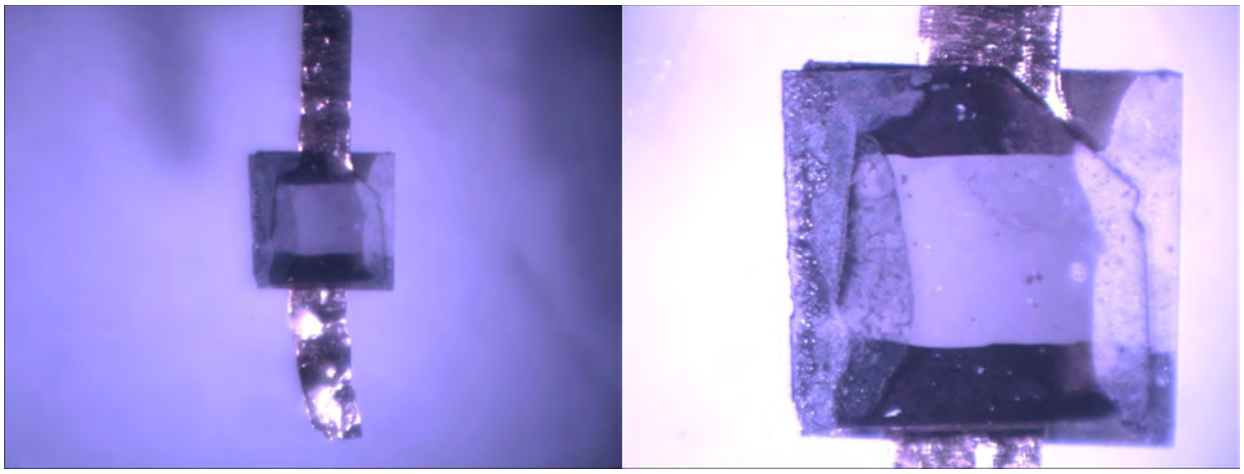

Figure 8. Sample assembly two diamond wafers compression bonded together with thick-film resistor applied; gold ribbons electrically connect the two diamond wafers together.

Pulsed Single-Layer Diamond Detector Measurements

An opportunity to take pulsed deuterium-deuterium fusion neutron measurements with the North Las Vegas DPF presented itself in Year Two of this project. The MAD detector team fielded the 5-µm-thick single-layer diamond detector for these measurements with the goal of observing charge multiplication while measuring a pulse of neutrons as opposed to a continuous neutron signal in the prior measurements. The detector as fielded is shown in Figure 8*a*.

The voltage signal as a function of time from the detector was collected for many DPF shots at three displacement field values: 10, 15, and 20 V/µm. The mean of the maximum voltage measured from each DPF shot was calculated at each of the three displacement field values and fitted with the Chynoweth model. The results of these measurements are shown in Figure 8*b*.

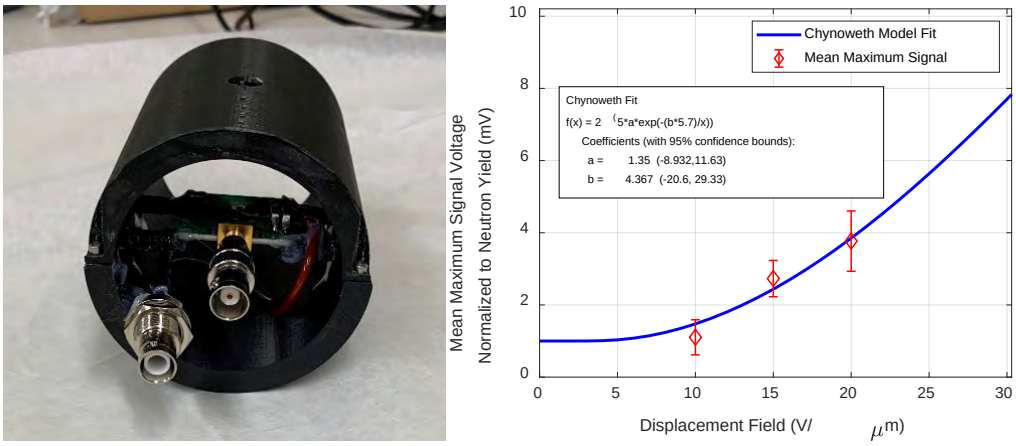

Figure 8. 5-µm-thick single-layer scCVD diamond detector as fielded on NLV DPF (*a*) and mean maximum voltage observed during each DPF shot of the measurement campaign as a function of displacement field fitted with Chynoweth model for charge multiplication (*b*).

The data do show an exponential behavior as the displacement field is increased. Furthermore, the mean maximum voltage at 15 V/μm was approximately 2.5 times greater than at 10 V/μm. At 20 V/μm, the mean maximum voltage was approximately 3.4 times greater than at 10 V/μm. This also indicates the presence of charge multiplication in the diamond increasing the output signal greater than what is expected simply by increasing the bias voltage (i.e., 1.5 times from 10 to 15 V/μm and 2 times from 10 to 20 V/μm).

Year Three: Fabrication and Testing of First Multi-Layered Diamond Detectors

Horizontal MAD Detector Fabrication

Applied Diamond faced ongoing challenges during the fabrication of the horizontal MAD detector so much so that their fabrication of the device continued well in to the third year of this project. This was despite having proved the individual fabrication processes on their own the prior year.

The first major challenge encountered was the passivation not adhering to the Au/Cr metallized electrodes on the diamond layer faces. Applied Diamond had demonstrated previously that the passivation could adhere directly to the diamond. They had also demonstrated that Au/Cr metallization adheres directly to the diamond (Au/Cr is their standard material combination for creating electrical contacts on diamond). However, their attempts at depositing the passivation on the Au/Cr metallized diamonds failed. They devised a solution using an alternative metallization and it worked.

The next challenge we faced was the application and curing of the thick-film resistor employed in the design of the horizontal MAD detector to provide the required resistance (tens of megaohms) to the electrodes. Applied Diamond practiced the delicate application of this thick film resistor on two surrogate diamond layers multiple times. What they discovered was that the application of the paste was difficult to control, and they had to use imprecise means to form the resistor. Artifacts of these difficulties can be seen in Figure 9 where the paste has flowed non-uniformly between the two diamond layers and Scotch tape (on the left of the diamond stack) was used in an attempt to control the width of the paste. Additional concerns regarding the thick film resistor included inability to precisely control the height of the paste which determined the resistance, breaking the very thin diamond layers during removal of the Scotch tape, and possible damage to the device and introduction of impurities during firing of the resistor in the vacuum furnace. These concerns were enough to investigate other resistive materials to replace the thick film resistor in our design.

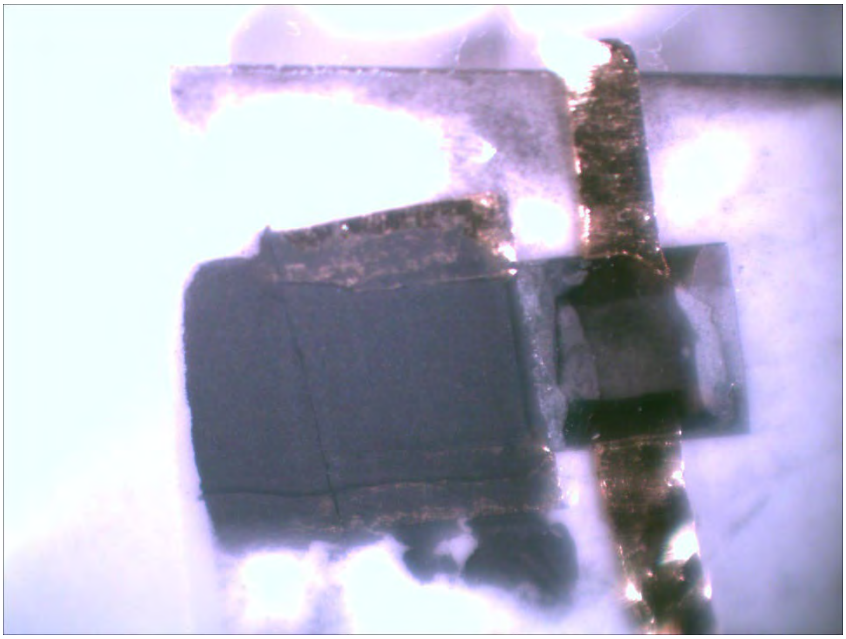

Figure 9. A later attempt at applying the thick film resistor to the horizontal MAD detector using Scotch tape to align and build-up the height of the resistor.

Applied Diamond suggested the use of a thin-film resistive contact. It was possible for a thin-film resistor to meet the resistance we required. Furthermore, the thin-film resistor could be sputtered on which allows for much more precise application on to the diamond layers. Based on the promise that thin-film resistor showed, we setup a subcontract late in the third year of this project for Applied Diamond to explore the feasibility of using thin-film resistor in lieu of the thick film resistor and they did. What they found was that thin-film resistor did indeed meet our target resistance. Applied Diamond went on to demonstrate the adhesion of the thin-film resistor to the diamond and the passivation. The thin-film resistor did not adhere well to the metallization.

The advantages of using the thin-film resistor over the thick film resistor were considerable with exception to the thin-film resistor's lack of adhesion to bare diamond. This issue alone did not deter our decision to move forward with the horizontal MAD detector using the thin-film resistor resistive material.

Choosing to move forward with the thin-film resistor meant that the horizontal MAD detector design had to change. To accommodate the thin-film resistor into the design with only two months left in the project, we simplified the horizontal MAD detector design to a single diamond layer. This single layer was still capable of showing considerable gain since the electric field was horizontal to the electrical contacts traversing the entire width of the diamond as opposed to the diamond thickness. Additional layers in the horizontal device will be attempted in future iterations. The vertical MAD detector demonstrates the capability to compression bond up to four diamond layers for now. Furthermore, since we already had two thinned, metallized, and passivated diamond chips, we decided to pursue to different approaches to adding the thin-film resistor.

The physical prototype implementing the original fine metallization pattern is shown in Figure 10. As of the writing of this report, the second physical prototype has not been received by the NNSS.

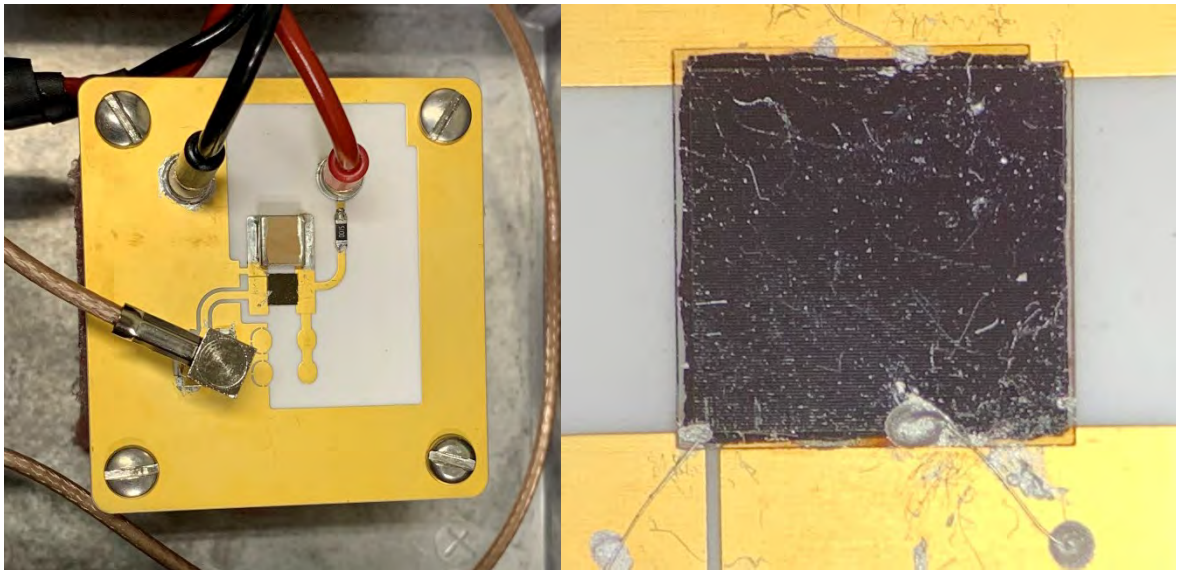

Figure 10. First prototype of the horizontal MAD detector–first alternative design; view of diamond on the printed circuit board (PCB) (*left*) and view zoomed in on diamond (*right*).

There were several issues noted upon inspection of the first horizontal MAD detector prototype that did not match our design. It appeared that there was no photomask used to apply the thin-film resistor to the diamond. Note the rough dark edges that indicate this in Figure 10. Applied Diamond indicated that they did use the photomask pattern we provided, but it does not appear this way. Another issue was the silver epoxy connecting the anode pad on the diamond to the printed circuit board (PCB). The silver epoxy not only contacts the anode, but also part of the electrode structure therefore shorting that connection. The last issue was the wire connecting the ground pad on the diamond to the PCB was loose. As of the writing of this report, the NNSS MAD detector team is working a solution to address the aforementioned issues. These issues will not be resolved before the end of the Site Directed Research and Development (SDRD) project.

Vertical MAD Detector Fabrication

The fabrication of the vertical MAD detector was much more straightforward, but indeed presented its own unique challenges.

The four 4 × 4 mm diamond layers making up the vertical MAD detector stack were laser cut and then thinned using a chemical etching process to achieve the targeted overall thickness. The diamond surfaces internal to the stack were metallized.

Our intended approach to assembling the four diamond layers together was to use compression bonding. Although we had proven this process in Year Two of this project, the vertical MAD detector design uses a much thinner metallization on the diamond surface than what was used

when we proved the process. When practicing for the final assembly of the vertical MAD detector prototype, the diamond layers would not adhere together because there was not enough metal between the diamond layers to fuse them together. An alternative approach using a clamp was pursued within the last few weeks of this project.

The clamped four diamond stack was then affixed to its NNSS-design printed circuit board and each individual diamond layer wired-bonded to it. Bias was supplied by means of a connection between the PCB and the bottom-most diamond's bottom metallized surface. As of the writing of this report, the vertical MAD detector prototype remains in transit to the NNSS.

Visit to Applied Diamond, Inc. in Wilmington, DE

The NNSS MAD detector team traveled out to Wilmington, DE, August 1–3, 2022 to visit the Applied Diamond leadership, staff, and facilities. Joe Tabeling, retired CEO and President, Victor Tabeling, current CEO and President, and Val Konovalov, Lead Scientist, participated in the discussions and tours with the NNSS MAD detector team. Photos from the team's visit are shown in Figure 11 and 12.

Figure 11. NNSS MAD detector team at the University of Delaware Nanofabrication Laboratory; from *left* to *right*–Robert Buckles, Kaleab Ayalew, Amber Guckes, and Adam Wolverton.

The NNSS and Applied Diamond teams had technical discussions on the current status, challenges, opportunities, and risks of both the horizontal and vertical MAD detector designs. At the conclusion of these discussions, we agreed on a path forward on both devices that was practical yet still achieved the ultimate goal of demonstrating multiplicative gain.

The two teams toured the Applied Diamond facilities including the diamond cutting, grinding, and polishing workspaces, the diamond growth reactors, the diamond metallization and lithography, and various diamond and diamond detector characterization apparatuses. The teams also visited the University of Delaware Nanofabrication Laboratory which consisted of a large

clean room host to the passivation and thin-film resistor targets used for photolithography on the horizontal MAD detector prototypes.

Figure 12. NNSS MAD detector principal investigator, Amber Guckes, discussing alternative approaches to the horizontal MAD detector design with Applied Diamond, Inc. retired CEO and President, Joe Tabeling, at the Applied Diamond facilities in Wilmington, DE.

Preparing for the Receipt of the First MAD Detector Prototypes

Prior to receiving the first MAD detector prototypes, we explored more deeply the polarization effect in diamond and different means to remedy it. We used a 500-µm-thick single-layer diamond detector for these measurements. Unfortunately, both the 5- and 10-µm-thick single-layer diamond detectors had previously experienced hard breakdowns rendering the detectors inoperable. With the 500-µm-thick diamond detector, it was observed that under progressive bias changes, it was susceptible to loss of performance due to polarization meaning we observed greater drift in the measured current and, thus, a greater standard deviation between measurements at the same bias voltage. The effect of polarization at biases below 100 V was minimal whereas the effects of polarization were more readily observed at higher bias voltages (up to 200 V).

Alternating the bias polarity prior to taking a measurement was one method that proved to mitigate the polarization effect especially below 150 V. However, at bias voltages greater than 150 V, the polarization effect could not be fully mitigated by alternating bias polarity alone. Alternating bias polarity followed by a short neutron irradiation proved to mitigate the polarization effect up to at least 200 V. The mean current and standard deviation measured over a range of bias voltages from +40 to +200 V using the aforementioned approaches to decreasing the effect of polarization are shown in Figure 13. It was the approach of alternating bias polarity with short neutron irradiation that was recommended for use to remedy polarization with the first MAD detector prototype direct current neutron measurements.

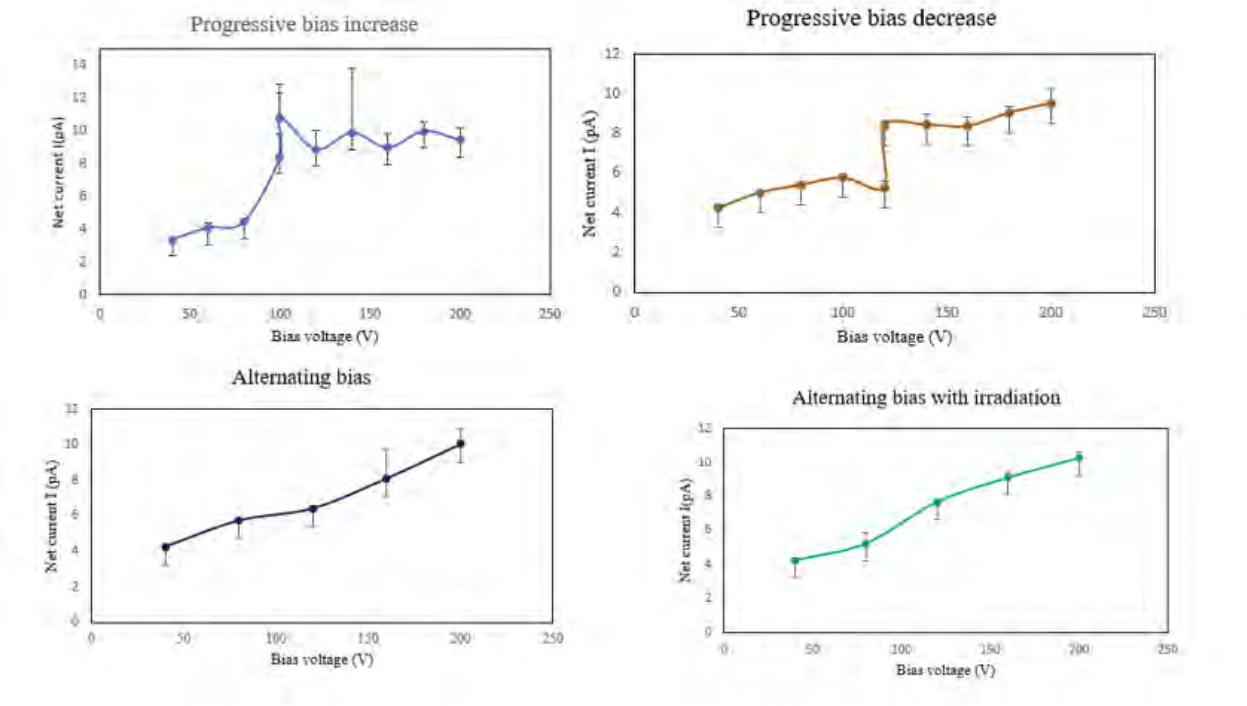

Figure 13. Net current measured from 500-µm scCVD diamond detector under various bias case scenarios. Error bar indicates standard deviation observed at each data point.

Direct Current Measurements of the First MAD Detector Prototypes

The first MAD detector prototypes were received during the last two weeks of this SDRD project. This did not leave the NNSS MAD detector team with enough time to perform direct current measurements characterizing the performance and gain of these devices.

Conclusion

Over the three years of the SDRD project, the NNSS MAD detector team has made tremendous progress towards the understanding of the avalanche effect in thin scCVD diamond and working towards delivery of the first MAD detector prototypes. This work will continue in FY 2023 under the support and funding of the NNSS Detectors & Instrumentation project. The team will start off the new year with the careful characterization of the prototypes and then will have an opportunity to field one of the MAD detector prototypes as a neutron in-beam diagnostic curing an NDSE static series campaign at the NNSS. The next iteration of the MAD detector design will be made based on the cumulative results of the FY 2023 efforts.

Significance

The MAD detector plays on the intrinsic avalanche and atomic properties of scCVD diamond to yield a novel fast neutron detector with inherent gain, improved detection efficiency compared to a single layer, and a small footprint. Such a device can provide an inherently low noise, high

fidelity, current mode measurement of a pulsed neutron source. This measurement is critical to informing the D-T DPF neutron source term in the calculation of the change in effective neutron multiplication factor, Δkeff, of test objects in the NNSS Area 11 DPF campaigns and ultimately the Excalibur series of SCEs.

Tie to Mission/Benefit

Emphasis on the advancement of neutron detection technologies was made at the most recent Mission Support and Test Services Neutron Detector System Workshop and in the FY 2022 NNSS R&D Technology Needs Assessment. High gamma ray rejection and intrinsic detection efficiency were called out as requirements important to the success of pulsed neutron experiments across the DOE complex including NDSE at the NNSS. The proposed MAD detector will meet these requirements and provide a low noise, high fidelity, current mode measurement of the neutron source term.

For NDSE, the measurement of the DPF neutron pulse is folded into the gamma-ray die-off signal measured by another set of detectors fielded for the experiment in order to calculate the Δk_{eff} of the interrogated target objects. The MAD detector fielded on this experiment as an in-beam neutron diagnostic would provide improved performance that would drive down the uncertainties for the fast detection diagnostic and ultimately the uncertainties in the calculation of Δk_{eff}. This is of critical importance to NDSE. The NDSE project leadership and scientists have shown interest in the MAD detector and have afforded our team the opportunity to field it on an NDSE static campaign in FY 2023.

The MAD detector can also enable nToF measurements on NDSE and other stockpile stewardship pulsed neutron experiments and contribute to spectroscopy capabilities for the Global Security mission.

Publications, Technology Abstracts

Green, J. A., A. Guckes, R. Buckles, D. Constantino, J. Friedman, J. Tabeling, A. Wolverton. 2020. “Geant4 and MCNP6.2 Modeling of Fast-Neutron Detectors Based on Single-Crystal Chemical Vapor Deposition Diamond.” *Proc. SPIE* **11494**: 1149417. https://doi.org/10.1117/12.2567750.

Guckes, A., R. Buckles, A. Wolverton, I. Garza, J. A. Green, J. Tabeling. 2021. “Direct current response of a thin scCVD diamond detector under increased applied field to 14.1 MeV neutrons.” *Proc. SPIE* **11838**: 1183814. https://doi.org/10.1117/12.2593455.

Guckes, A., R. Buckles, J.A. Green, A. Wolverton. 2020. “Multi-Layered Avalanche Diamond Detector for Fast Neutron Applications.” Technology Abstract, Las Vegas, NV: Mission Support and Test Services, LLC.

TRL Start and End

The technical readiness level (TRL) of the MAD detector started at TRL 1, basic principles established, at the start of Year One of this SDRD project. It ended at the completion of Year Three at TRL 4, ready for prototype lab testing.

Acknowledgments

We would like to thank Joe Tabeling and Val Konovalov of Applied Diamond, Inc. for working so closely with us over the past three weeks in making the first MAD detector prototypes a reality. Joe met with us every 2-3 weeks throughout the project in which he would update us on the status of our devices and help us brainstorm solutions to challenges that came up (and they came up often). Joe, together with Val, told us when our ideas were outlandish and impossible and provided invaluable insight to make our ideas feasible.

We would also like to thank Irene Garza and Steve Pennock for enabling the neutron measurements at the North Las Vegas Source Range Laboratory. Irene's extraordinary experience with radiation detectors and sources allowed us to collect excellent data on our early single-layer diamond detectors and on our first MAD detector prototypes. Of course, Steve kept us safe from the neutrons.

Thank you to the North Las Vegas Dense Plasma Focus team and Danny Lowe for allowing us to piggy-back on DPF shots so that we could collect pulse current mode data on our single-layer diamond detectors. This exact application is where we intend the MAD detector to end up: as a neutron source term diagnostic for the DPF fielded on NDSE.

Our last thank you, to the SDRD program for giving this project a chance, we are forever grateful for you believing in our idea and in us. It has been so fulfilling to see it start as an idea and then to see that idea become a reality. We are certainly not done yet.

References

Antula, J. 1972. "Experimental Evidence of Hot-Electron Transport through Thin Metal Films." *J Appl Phys.* **43**: 1830. https://doi.org/10.1063/1.1661404.

Bennett, P., A. Kargar, L. Cirignano, H. Kim, K. Shah. 2018. "CVD Diamond for Beta Particle Detection in a Gamma-Ray Background." *Proc. SPIE Volume 10762, Hard X-Ray, Gamma-Ray, and Neutron Detector Physics XX*: 107620Z. https://doi.org/10.1117/12.2323695.

Chynoweth, A. G. 1958. "Ionization Rates for Electrons and Holes in Silicon." *Phys Rev*. **109** (5): 1537. https://doi.org/10.1103/PhysRev.109.1537.

Dueñas, J. A., J . M. Mora, M. Traeger, A. Galbiati, I. Martel, E. Berdermann. 2015. "Time Response of 50 μm Thickness Single Crystal Diamond Detectors." *Diam Relat Mater*. **55**: 144–148. https://doi.org/10.1016/j.diamond.2015.03.018.

Evaluated Nuclear Data File (ENDF) (version ENDF/B-VIII.0, February 2, 2018, accessed June 21, 2022). Brookhaven National Laboratory, National Nuclear Data Center. https://www.nndc.bnl.gov/endf/.

Gabrysch, M. 2010. "Charge Transport in Single-Crystalline CVD Diamond." *Digital Comprehensive Summaries of Uppsala Dissertations from the Faculty of Science and Technology*. Uppsala, Sweden: Acta Universitatis Upsaliensis.

Kania, D. R., M. I. Landstrass, M. A. Piano, L. S. Pan, S. Han. 1993. "Diamond Radiation Detectors." *Diam Relat Mater*. **2** (5–7): 1012–1019. https://doi.org/10.1016/0925-9635(93)90266-5.

Knoll, G.F. 2010. *Radiation Detection and Measurements*, 4th ed. John Wiley & Sons: Hoboken, NJ.

Monteblanco, E., F. Donatini, M. Hehn, D. Lacour, Y. Lassailly, J. Pretti, N. Rougemaille. 2019. "Tranmission of High-Energy Electrons through Metal Semiconductor Schottky Junctions." *Phys Rev B*. **100**: 205301. https://journals.aps.org/prb/abstract/10.1103/PhysRevB.100.205301.

Muškinja, M., V. Cindro, A. Gorišek, H. Kagan, G. Kramberger, I. Mandić, M. Mikuž, S. Phan, D. S. Smith, M. Zavrtanik. 2017. "Investigation of charge multiplication in single crystalline CVD diamond particle detectors," *Nucl Instrum Methods Phys Res A*. **841**: 162–169; https://doi.org/10.1016/j.nima.2016.10.018.

Nebel, C. 2003. "Electronic Properties of CVD Diamond." *Semicon Sci Technol*. **18** (3): S1. https://doi.org/10.1088/0268-1242/18/3/301.

Schmid, G. J., J. A. Koch, R. A. Lerche, M. J. Moran. 2014. "A Neutron Sensor Based on Single Crystal CVD Diamond," *Nucl Instrum Methods Phys Res A*. **527**: 554–561. https://doi.org/10.1016/j.nima.2004.03.199.

Skukan, N. et al. 2016. "Charge Multiplication Effect in Thin Diamond Films." *Appl Phys Lett*. **109**: 043502. https://doi.org/10.1063/1.4959863.